Research Article | Vol. 9, No. 7 | 1 Jul 2018 | BIOMEDICAL OPTICS EXPRESS 3193
Biomedical Optics EXPRESS

Prediction of the anti-glioma therapeutic effects of temozolomide through *in vivo* molecular imaging of MMP expression

LI LI,[1,2,3] YANG DU,[3,5] DEHUI XIANG,[1,2] LIANG CHEN,[4] ZHIFENG SHI,[4] JIE TIAN,[3,6] AND XINJIAN CHEN[1,2,7]

[1]*School of Electronic and Information Engineering, Soochow University, No. 1 Ten Azusa Street, Suzhou, 215006, China*
[2]*State Key Laboratory of Radiation Medicine and Protection, School of Radiation Medicine and Protection, Soochow University, Suzhou, 215123, China*
[3]*CAS Key Laboratory of Molecular Imaging, The State Key Laboratory of Management and Control for Complex Systems, Institute of Automation, Chinese Academy of Sciences, No. 95 Zhongguancun East Road, Haidian District, Beijing, 100190, China*
[4]*Department of Neurosurgery, Huashan Hospital, Fudan University, No. 12 Urumqi Road, Jingan District, Shanghai, 200040, China*
[5]*yang.du@ia.ac.cn*
[6]*tian@ieee.org*
[7]*xjchen@suda.edu.cn*

Abstract: Currently, there is no effective way to assess the therapeutic response of temozolomide (TMZ) for the glioma. In this study, the human U87MG-fLuc glioma animal models were set up and the antitumor efficacy of TMZ was evaluated using bioluminescence imaging (BLI) and MRI. Then, bioluminescence tomography (BLT) was reconstructed using an adaptive sparsity matching pursuit (ASMP) algorithm. Second, the expression level of the MMP-750 probe was examined with or without TMZ treatment using FMI. Third, the expression of MMP2 and MMP3 was specifically examined after treatment. The results showed that TMZ effectively inhibited glioma growth. The targeted imaging of MMP-750 was decreased during the treatment of glioma with TMZ. Moreover, the MMP2 and MMP3 expression was found to correlate with the inhibition effect of TMZ. Our study indicated that the therapeutic effects of TMZ can be effectively evaluated at an early stage using molecular imaging, and MMP targeting the fluorescence probe could be utilized for the prediction and assessment of the therapeutic effects of TMZ.

OCIS codes: (170.3880) Medical and biological imaging; (110.6955) Tomographic imaging; (170.6280) Spectroscopy, fluorescence and luminescence; (170.4580) Optical diagnostics for medicine.

References and links

1. R. Stupp, W. P. Mason, M. J. van den Bent, M. Weller, B. Fisher, M. J. Taphoorn, K. Belanger, A. A. Brandes, C. Marosi, U. Bogdahn, J. Curschmann, R. C. Janzer, S. K. Ludwin, T. Gorlia, A. Allgeier, D. Lacombe, J. G. Cairncross, E. Eisenhauer, and R. O. Mirimanoff, "Radiotherapy plus concomitant and adjuvant temozolomide for glioblastoma," N. Engl. J. Med. **352**(10), 987–996 (2005).
2. E. G. Van Meir, C. G. Hadjipanayis, A. D. Norden, H. K. Shu, P. Y. Wen, and J. J. Olson, "Exciting New Advances in Neuro-Oncology: the avenue to a cure for malignant glioma," CA Cancer J. Clin. **60**(3), 166–193 (2010).
3. P. K. Kornblith, W. C. Welch, and M. K. Bradley, "The future of therapy for glioblastoma," Surg. Neurol. **39**(6), 538–543 (1993).
4. E. Galanis and J. Buckner, "Chemotherapy for high-grade gliomas," Br. J. Cancer **82**(8), 1371–1380 (2000).
5. M. Brada, and M. Prados (ed). Brain Cancer," Ann Oncol **13**, 1511 (2002).
6. T. Kanzawa, I. M. Germano, T. Komata, H. Ito, Y. Kondo, and S. Kondo, "Role of autophagy in temozolomide-induced cytotoxicity for malignant glioma cells," Cell Death Differ. **11**(4), 448–457 (2004).
7. H. Kurzen, S. Schmitt, H. Näher, and T. Möhler, "Inhibition of angiogenesis by non-toxic doses of temozolomide," Anticancer Drugs **14**(7), 515–522 (2003).

#326861 https://doi.org/10.1364/BOE.9.003193
Journal © 2018 Received 29 Mar 2018; revised 4 May 2018; accepted 21 May 2018; published 20 Jun 2018

Biomedical Optics EXPRESS

8. M. Brada, K. Hoang-Xuan, R. Rampling, P. Y. Dietrich, L. Y. Dirix, D. Macdonald, J. J. Heimans, B. A. Zonnenberg, J. M. Bravo-Marques, R. Henriksson, R. Stupp, N. Yue, J. Bruner, M. Dugan, S. Rao, and S. Zaknoen, "Multicenter phase II trial of temozolomide in patients with glioblastoma multiforme at first relapse," Ann. Oncol. **12**(2), 259–266 (2001).
9. M. Brada, I. Judson, P. Beale, S. Moore, P. Reidenberg, P. Statkevich, M. Dugan, V. Batra, and D. Cutler, "Phase I dose-escalation and pharmacokinetic study of temozolomide (SCH 52365) for refractory or relapsing malignancies," Br. J. Cancer **81**(6), 1022–1030 (1999).
10. M. F. Stevens, J. A. Hickman, S. P. Langdon, D. Chubb, L. Vickers, R. Stone, G. Baig, C. Goddard, N. W. Gibson, and J. A. Slack, *Antitumor activity and pharmacokinetics in mice of 8-carbamoyl-3-methyl-imidazo[5,1-d]-1,2,3,5-tetrazin-4(3H)-one (CCRG 81045; M & B 39831), a novel drug with potential as an alternative to dacarbazine* (William B. Eerdmans, 1987), pp. 5846–5852.
11. W. K. Yung, M. D. Prados, R. Yaya-Tur, S. S. Rosenfeld, M. Brada, H. S. Friedman, R. Albright, J. Olson, S. M. Chang, A. M. O'Neill, A. H. Friedman, J. Bruner, N. Yue, M. Dugan, S. Zaknoen, and V. A. Levin, "Multicenter phase II trial of temozolomide in patients with anaplastic astrocytoma or anaplastic oligoastrocytoma at first relapse," J. Clin. Oncol. **17**(9), 2762–2771 (1999).
12. W. K. A. Yung, R. E. Albright, J. Olson, R. Fredericks, K. Fink, M. D. Prados, M. Brada, A. Spence, R. J. Hohl, W. Shapiro, M. Glantz, H. Greenberg, R. G. Selker, N. A. Vick, R. Rampling, H. Friedman, P. Phillips, J. Bruner, N. Yue, D. Osoba, S. Zaknoen, and V. A. Levin, "A phase II study of temozolomide vs. procarbazine in patients with glioblastoma multiforme at first relapse," Br. J. Cancer **83**(5), 588–593 (2000).
13. C. H. Contag and M. H. Bachmann, "Advances in *in vivo* bioluminescence imaging of gene expression," Annu. Rev. Biomed. Eng. **4**(1), 235–260 (2002).
14. A. McCaffrey, M. A. Kay, and C. H. Contag, "Advancing molecular therapies through *in vivo* bioluminescent imaging," Mol. Imaging **2**(2), 75–86 (2003).
15. V. Ntziachristos, J. Ripoll, L. V. Wang, and R. Weissleder, "Looking and listening to light: the evolution of whole-body photonic imaging," Nat. Biotechnol. **23**(3), 313–320 (2005).
16. A. Rehemtulla, L. D. Stegman, S. J. Cardozo, S. Gupta, D. E. Hall, C. H. Contag, and B. D. Ross, "Rapid and quantitative assessment of cancer treatment response using *in vivo* bioluminescence imaging," Neoplasia **2**(6), 491–495 (2000).
17. A. Söling and N. G. Rainov, "Bioluminescence imaging *in vivo* - application to cancer research," Expert Opin. Biol. Ther. **3**(7), 1163–1172 (2003).
18. J. C. Wu, I. Y. Chen, G. Sundaresan, J. J. Min, A. De, J. H. Qiao, M. C. Fishbein, and S. S. Gambhir, "Molecular imaging of cardiac cell transplantation in living animals using optical bioluminescence and positron emission tomography," Circulation **108**(11), 1302–1305 (2003).
19. G. Wang, W. Cong, Y. Li, and W. Han, "Recent development in bioluminescence tomography," IEEE Int Symp Biomed Imaging **2**, 678–681 (2006).
20. G. Wang, Y. Li, and M. Jiang, "Uniqueness theorems in bioluminescence tomography," Med. Phys. **31**(8), 2289–2299 (2004).
21. C. Bremer, C. H. Tung, and R. Weissleder, "*In vivo* molecular target assessment of matrix metalloproteinase inhibition," Nat. Med. **7**(6), 743–748 (2001).
22. M. Egeblad and Z. Werb, "New functions for the matrix metalloproteinases in cancer progression," Nat. Rev. Cancer **2**(3), 161–174 (2002).
23. A. F. Chambers and L. M. Matrisian, "Changing Views of the Role of Matrix Metalloproteinases in Metastasis," J. Natl. Cancer Inst. **89**(17), 1260–1270 (1997).
24. L. J. McCawley and L. M. Matrisian, "Matrix metalloproteinases: they're not just for matrix anymore!" Curr. Opin. Cell Biol. **13**(5), 534–540 (2001).
25. M. L. Lamfers, D. Gianni, C. H. Tung, S. Idema, F. H. Schagen, J. E. Carette, P. H. Quax, V. W. Van Beusechem, W. P. Vandertop, C. M. Dirven, E. A. Chiocca, and W. R. Gerritsen, "Tissue inhibitor of metalloproteinase-3 expression from an oncolytic adenovirus inhibits matrix metalloproteinase activity *in vivo* without affecting antitumor efficacy in malignant glioma," Cancer Res. **65**(20), 9398–9405 (2005).
26. M. E. Stearns and M. Wang, "Type IV collagenase (M(r) 72,000) expression in human prostate: benign and malignant tissue," Cancer Res. **53**(4), 878–883 (1993).
27. B. Davies, J. Waxman, H. Wasan, P. Abel, G. Williams, T. Krausz, D. Neal, D. Thomas, A. Hanby, and F. Balkwill, "Levels of matrix metalloproteases in bladder cancer correlate with tumor grade and invasion," Cancer Res. **53**(22), 5365–5369 (1993).
28. S. Zucker, M. Hymowitz, C. Conner, H. M. Zarrabi, A. N. Hurewitz, L. Matrisian, D. Boyd, G. Nicolson, and S. Montana, "Measurement of Matrix Metalloproteinases and Tissue Inhibitors of Metalloproteinases in Blood and Tissues. Clinical and Experimental Applications," Ann. N. Y. Acad. Sci. **878**, 212–227 (1999).
29. M. A. Moses, D. Wiederschain, K. R. Loughlin, D. Zurakowski, C. C. Lamb, and M. R. Freeman, "Increased incidence of matrix metalloproteinases in urine of cancer patients," Cancer Res. **58**(7), 1395–1399 (1998).
30. J. Fang, Y. Shing, D. Wiederschain, L. Yan, C. Butterfield, G. Jackson, J. Harper, G. Tamvakopoulos, and M. A. Moses, "Matrix Metalloproteinase-2 Is Required for the Switch to the Angiogenic Phenotype in a Tumor Model," Proc. Natl. Acad. Sci. U.S.A. **97**(8), 3884–3889 (2000).
31. A. Kwiatkowska, M. Kijewska, M. Lipko, U. Hibner, and B. Kaminska, "Downregulation of Akt and FAK phosphorylation reduces invasion of glioblastoma cells by impairment of MT1-MMP shuttling to lamellipodia and downregulates MMPs expression," Biochim. Biophys. Acta **1813**(5), 655–667 (2011).

Biomedical Optics EXPRESS

32. Q. Li, B. Chen, J. Cai, Y. Sun, G. Wang, Y. Li, R. Li, Y. Feng, B. Han, J. Li, Y. Tian, L. Yi, and C. Jiang, "Comparative Analysis of Matrix Metalloproteinase Family Members Reveals That MMP9 Predicts Survival and Response to Temozolomide in Patients with Primary Glioblastoma," PLoS One **11**(3), e0151815 (2016).
33. P. S. Smith-Pearson, E. K. Greuber, G. Yogalingam, and A. M. Pendergast, "Abl kinases are required for invadopodia formation and chemokine-induced invasion," J. Biol. Chem. **285**(51), 40201–40211 (2010).
34. I. Ulasov, B. Thaci, P. Sarvaiya, R. Yi, D. Guo, B. Auffinger, P. Pytel, L. Zhang, C. K. Kim, A. Borovjagin, M. Dey, Y. Han, A. Y. Baryshnikov, and M. S. Lesniak, "Inhibition of MMP14 potentiates the therapeutic effect of temozolomide and radiation in gliomas," Cancer Med. **2**(4), 457–467 (2013).
35. H. Wu and S. Wang, "Adaptive Sparsity Matching Pursuit Algorithm for Sparse Reconstruction," IEEE Signal Process. Lett. **19**(8), 471–474 (2012).
36. H. Hu, J. Liu, L. Yao, J. Yin, N. Su, X. Liu, F. Cao, J. Liang, Y. Nie, and K. Wu, "Real-time bioluminescence and tomographic imaging of gastric cancer in a novel orthotopic mouse model," Oncol. Rep. **27**(6), 1937–1943 (2012).
37. J. J. Killion, R. Radinsky, and I. J. Fidler, "Orthotopic models are necessary to predict therapy of transplantable tumors in mice," Cancer Metastasis Rev. **17**(3), 279–284 (1998).
38. M. Edinger, Y. A. Cao, M. R. Verneris, M. H. Bachmann, C. H. Contag, and R. S. Negrin, "Revealing lymphoma growth and the efficacy of immune cell therapies using *in vivo* bioluminescence imaging," Blood **101**(2), 640–648 (2003).
39. M. Folaron and M. Seshadri, "Bioluminescence and MR Imaging of the Safety and Efficacy of Vascular Disruption in Gliomas," Mol. Imaging Biol. **18**(6), 860–869 (2016).
40. C. Galiger, M. Brock, G. Jouvion, A. Savers, M. Parlato, and O. Ibrahim-Granet, "Assessment of efficacy of antifungals against Aspergillus fumigatus: value of real-time bioluminescence imaging," Antimicrob. Agents Chemother. **57**(7), 3046–3059 (2013).
41. T. Demuth and M. E. Berens, "Molecular mechanisms of glioma cell migration and invasion," J. Neurooncol. **70**(2), 217–228 (2004).
42. J. Gross and C. M. Lapiere, "Collagenolytic activity in amphibian tissues: a tissue culture assay," Proc. Natl. Acad. Sci. U.S.A. **48**(6), 1014–1022 (1962).
43. S. Curran and G. I. Murray, "Matrix metalloproteinases: molecular aspects of their roles in tumour invasion and metastasis," Eur. J. Cancer **36**(13), 1621–1630 (2000).
44. L. A. Liotta, K. Tryggvason, S. Garbisa, I. Hart, C. M. Foltz, and S. Shafie, "Metastatic potential correlates with enzymatic degradation of basement membrane collagen," Nature **284**(5751), 67–68 (1980).
45. H. Nagase and J. F. Woessner, Jr., "Matrix metalloproteinases," J. Biol. Chem. **274**(31), 21491–21494 (1999).
46. A. R. Nelson, B. Fingleton, M. L. Rothenberg, and L. M. Matrisian, "Matrix metalloproteinases: biologic activity and clinical implications," J. Clin. Oncol. **18**(5), 1135–1149 (2000).
47. B. Shrestha and S. Subedi, "Matrix Metalloproteinase," Curr. Opin. **84**, 160 (1997).

1. Introduction

Malignant gliomas are one of the most intractable and fatal cancers due to their location, aggressive biological behavior and invasive growth [1, 2]. Although neuroimaging and chemotherapy have made rapid progress in modern times, it is difficult for cancer patients to recover completely [3]. Glioma shows certain resistance to many chemotherapy agents (e.g., nitrosourea or the combination regimen procarbazine, lomustine and vincristine) [4]. Even if the blood-brain barrier is broken down in glioma patients, most chemotherapeutic drugs do not effectively infiltrate the brain [5].

Temozolomide (TMZ) is a novel imidazotetrazinone methylating agent. TMZ is a small lipophilic molecule and it can effectively cross the blood-brain barrier [6, 7]. TMZ has shown a schedule-dependent antitumor activity in malignant gliomas [8–12]. TMZ is commonly used to treat malignant brain tumors; currently there is no effective way for monitoring and evaluating TMZ treatment effects at the early stage. Medical imaging technologies, as computed x-ray tomography (CT), ultrasound (US) and magnetic resonance imaging (MRI), play an indispensable role in clinical practice. However, these imaging methods usually detect cancer in areas that are a centimeter or larger in diameter, at which point patients are difficult to cure. There are tremendous incentives to develop novel imaging technologies for the early detection of cancer. In comparison with traditional anatomical imaging methods, molecular imaging is unique in specificity and sensitivity. Molecular imaging has important clinical value in predicting the anti-tumor effect of drugs. It becomes an important imaging tool to diagnose diseases, evaluate therapeutic efficacies, and facilitate drug development and other biomedical applications as well [13–18]. However, such two-dimensional bioluminescence imaging is incapable to provide 3-dimensional information of

Biomedical Optics EXPRESS

internal features of interest, and does not reveal in-depth information. Bioluminescence tomography (BLT) reconstructs an internal bioluminescent source distribution from external optical measures which can be localized and quantified in 3D [19, 20], and BLT allows the integration of molecular and physiological information with anatomical information.

Proteinases endow tumor cells with the ability to invade and metastasize to different tissue sites *in vivo* [21]. Matrix metalloproteinases (MMPs), a family of calcium-dependent endopeptidases [22], have been identified as one of the major proteinase systems responsible for extracellular proteolysis. MMPs enable tumor cells to break through basement membranes and invade [23]. MMPs promote tumor cell invasion by degrading extracellular-matrix proteins, and activating signal-transduction pathways [24]. MMP activity in the tumor environment was dynamically assessed by using an MMPSense 750 imaging probe. MMPSense 750 was quenched with near-infrared fluorochromes positioned on a non-immunogenic backbone previously designed as to sense proteinase activities directly *in vivo* in intact tumor environments [21]. This probe is a metalloprotease substrate, optically silent in its inactive state and highly fluorescent following MMP-mediated activation [21, 25]. Our previous work indicates that MMP-750 can specifically target gliomas and fluorescence tomography (FMT) of MMP-750 provides 3D information for the spatial localization of gliomas *in situ*, and hence works as an ideal fluorescence probe for gliomas.

The expression level of some MMPs in cancer tissues is higher than that in normal tissues and the extent of expression is related to the tumor stage [26], invasiveness [27, 28], metastasis [29] and angiogenesis [30]. Moreover, it is reported that the expression of MMP family members are highly expressed in gliomas, and the expression levels are related to TMZ treatment [31–34]. Hence, it is interesting to study whether targeted imaging of MMP-750 probes can predict antitumor activities of TMZ therapy. Moreover, it is known that MMPSense 750 can be activated by a series of MMPs, but which specific MMP members are functional for the regulation of TMZ treatment is still not known.

The aims of this work are to investigate the treatment effects of TMZ using BLT on both xenograft and orthotopic glioma mouse models; second, the FMI of gliomas using an MMP-750 probe was studied during TMZ treatment. Finally, the expression of MMPs specifically correlated with the treatment efficacy of TMZ was studied using western blot and immunohistochemistry (IHC) experiments.

2. Materials and methods

2.1 Materials and reagents

A human U87MG-fLuc glioma cell line was obtained from the American type culture collection (ATCC). Culturing medium and fetal bovine serum (FBS) were purchased from HyClone (Thermo Scientific, USA). D-Luciferin was bought from Biotium (CA, Fremont, USA). Temozolomide (TMZ) was obtained from Schering-Plough Corporation (Kenilworth, NJ, USA). The TMZ solution (0.5 mg/μl) was prepared in dimethyl sulfoxide (DMSO). Before the injection, the stock drug solution was thawed, diluted in sterile saline to a final concentration of 0.005 mg/μl. MMP-750 was purchased from PerkinElmer (Waltham, MA, USA). The emission spectra peak was 775 nm, and excitation spectra peak was 749 nm.

2.2 Cell culture

U87MG-fLuc is a human GBM cell line. Cells were grown in Dulbecco's modified eagle medium and supplemented with 10% fetal bovine serum (FBS), and were maintained under a humidified atmosphere of 5% CO_2 at 37°C.

2.3 Mouse glioma models

The experiments were carried out in male BALB/c athymic nude mice, 4-5 weeks (Vital River Laboratory Animal Technology Corporation, Beijing, China). The mice were

Biomedical Optics EXPRESS

maintained under specific-pathogen-free conditions in accordance with the guidelines of the Institutional Animal Care and Use Committee (IACUC) at Peking University (Permit No: 2011-0039). The experiments were carried out in accordance with the approved guidelines. The U87MG xenograft animal models were inoculated with 10^7 U87MG cells. Only single-cell suspensions with >90% viability were used for injections. The mice were randomly divided into two groups (n = 10 for control group and n = 10 for TMZ group). For TMZ group, animals received six doses of TMZ (50 mg/kg/day) on consecutive days, starting 6 days after tumor inoculation. At the same time, however, the control group was given an equal amount of 0.9% saline i.p. The tumor volume was measured with calipers as follows:

$$v = 1/2\, xy^2 \tag{1}$$

where v is the tumor size, x is the large diameter of the tumor, and y is the small diameter of the tumor. At the same time, the weight and survival of mice were recorded during the experiment.

The orthotopic tumor bearing mice (N = 20) were anesthetized by i.p. injection of sodium pentobarbital. After disinfection and incision of the skin, a small hole was made in the skull through the skin overlying the cranium. The mice were stationed in a stereotactic frame with an ear bar. About 10^6 glioma cells in a volume of 4 μl PBS were injected slowly into the brain, and then the scalp was closed with sutures. A Hamilton syringe (Anting Co. Shanghai, China) attached to the stereotaxic system was used to implant all of the tumor cells.

2.4 TMZ treatment

Ten days after tumor inoculation, the mice were randomly divided into two groups (n = 10 for the control group and n = 10 for the TMZ group). The TMZ and control groups were administered TMZ i.p. (50 mg/kg/day) and an equal amount of 0.9% saline for 6 days, respectively. The mouse body weight and tumor volume were recorded every five days. To obtain the data, the survival rates were monitored daily and mice were euthanized at the appearance of severe neurological damage from tumor growth.

2.5 Magnetic resonance imaging (MRI)

Mice were required to be anesthetized for the image acquisition. Mice were lightly anesthetized with 2% isoflurane mixed with oxygen using a vaporizer (Lumic International). To assess the tumor size, mice underwent MRI scanning on the 10th day after completion of drug treatment. T1-weighted MRI images were obtained with a compact high-performance MRI system (1.5T, M3TM, Aspect Imaging, Israel) after injection of 0.1 ml contrast medium (Gadodiamide, Omniscan, Amersham) into the tail vein. *In vivo* multi-slice images of mouse brains were acquired in the axial plane (TR 6000 ms, TE 50 ms, slice thickness 0.8 mm and slice spacing 0.2 mm).

2.6 In vivo *bioluminescent imaging (BLI)*

For the sake of evaluating the antitumor efficacy of TMZ, BLI of the glioma-bearing mice was acquired every 5 days after treatment began. Before BLI was acquired, the mice were anesthetized and injected with D-luciferin i.p. (150 mg/kg) for 8 minutes. The data were collected with an IVIS Spectrum Imaging System (PerkinElmer, Germany).

2.7 Fluorescence imaging (FMI) of MMP-750

The MMP-750 probe was reconstituted with 1.2 mL of 1 × phosphate-buffered saline (PBS) before intravenous injection of animals at a dose of 2 nmol (100μL) per mouse. The *in vivo* bio-distribution of the MMP-750 probe was dynamically monitored using the IVIS Spectrum Imaging System (PerkinElmer, USA) at different time points after intravenous injection.

Biomedical Optics EXPRESS

2.8 Micro-CT/BLI system

Bioluminescence tomography (BLT) was studied and reconstructed using BLI and CT data. The schematics of the Micro-CT/BLI system are shown in Fig. 1. The Micro-CT system consists of a micro-focus X-ray source (UltraBright, Oxford Instruments, USA). The maximum output power of the X-ray tube is 80 W. The X-ray flat panel detector (C7942CA-02, Hamamatsu, Japan) had a 120 mm × 120 mm photodiode area. In addition, there is a charge-coupled device (CCD) camera (VersArray, Princeton Instruments, Trenton, New Jersey) on the turntable. Images were taken with the CCD camera, cooled down to –80°C, with a chip size of 1,024 × 1,024 pixels. The distance between the lens and the mice was adjusted for best image clarity. It is worth mentioning that they were all mounted on a vertical electric turntable rotating at a uniform speed under computer control. The multimodal imaging system was located in a light-tight enclosure made of a tinplate, which can block all kinds of visible light and rays from the surrounding environment.

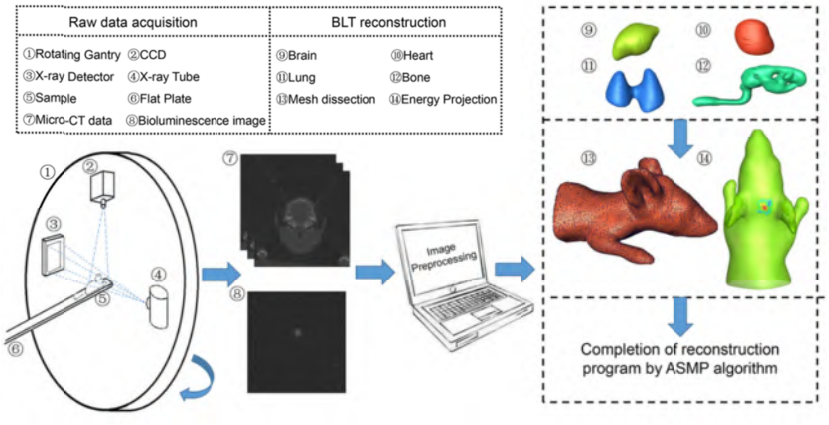

Fig. 1. The schematic of the Micro-CT/BLI system and the data processing procedure.

2.9 In vivo BLT imaging of an orthotopic mouse glioma

BLT was implemented to the orthotopic tumor mouse models on the 7th day after completion of drug treatment. The mice were anesthetized with 2% isoflurane and injected i.p. with D-luciferin (150 mg/kg) for 8 minutes. The anesthetized mice were placed and fixed to a flat plate perpendicular to the turntable. The BLI signal was acquired, and then 3D anatomical data were obtained using the Micro-CT system.

2.10 Reconstruction method

The data processing procedure is shown in Fig. 1. Firstly, the anatomical structure of knowledge is established from the micro-CT scans. The micro-CT image volume of the mice was partitioned semi-automatically into major biological tissues, including brain, lung, heart and bone. Secondly, the geometrical model was established for the mouse body as the region of interest consisting of 3862 nodes and 18692 tetrahedrons using software Amira 5.2.1 (Mercury Computer Systems, Inc. Chelmsford, MA). Thirdly, the bioluminescence data were mapped onto the surface of the geometrical model. After preprocessing of the measured data, the results of registration and mesh generation were both performed to solve an implementation of BLT by rebuilding the algorithm. From the perspective of compressed sensing, tumor reconstruction was conducted as a problem of sparse signal recovery. Hence, an adaptive sparsity matching pursuit (ASMP) method is presented for BLT reconstruction [35]. ASMP can refine the chosen supports and extract sparse information automatically,

Biomedical Optics EXPRESS

compared to the general subspace pursuit algorithms, which enhances the reconstruction accuracy and robustness.

The procedure of the proposed algorithm was as follows:

Algorithm 1: Adaptive Sparsity Matching Pursuit (ASMP)

Input: $A-M\times N$ matrix, y -measurements vector, $N_{\max}$ -the number of maximum iterations allowed.

Initialization: $\hat{x}=0$, the residual $r=y$

Outer iteration:

compute the signal proxy $v=A^{T}r$

form the index set $\Omega=\{j:|v(j)|>\tau\|r\|_2/\sqrt{M}\}$

sparsity estimation $s=\left\|\Omega\bigcup supp(\hat{x})\right\|_0$

inner counter $k=1$

$r^{(0)}=r$, $x^{(0)}=\hat{x}$

Inner iteration:

identify supports $u=A^{T}r^{(k-1)}$, $\Lambda=supp(u_s)$

form the supporting set $\Gamma=\Lambda\bigcup supp(x^{(k-1)})$

least squares (LS) estimation $b=\arg\min_{x':supp(x'=\Gamma)}\left\|Ax'-y\right\|_2$

prune the estimate $x^{(k)}=b_s$

update residual $r^{(k)}=y-Ax^{(k)}$

$\left\|r^{(k)}\right\|_2\le\left\|r^{(k-1)}\right\|_2$, then

$k=k+1$

Else

$r=r^{(k-1)}$

$\hat{x}=x^{(k-1)}$

quit the inner iteration

End if

End inner iteration

If halting condition true $n\ge N_{\max}$ then

quit the outer iteration

End if

End outer iteration

Output: Approximation $\hat{x}$.

where $supp(x)=\{i:x_i\neq 0\}$, s is the estimated sparsity, Ω, Λ and Γ are the subsets of $\{1,2,...,N\}$, and x_s denotes the s-largest components of x. $\tau=3$.

2.11 Real-time PCR of MMP2 and MMP3 after treatment with TMZ

U87MG tumor cells were cultured in vitro and treated with different concentrations of TMZ. RNA was extracted and cDNA was synthesized. The forward primer for MMP2 was GATACCCCTTTGACGGTAAGGA, and reverse primer was CCTTCTCCCAAGGTCCATAGC; the forward primer for MMP3 was

Biomedical Optics EXPRESS

AGTCTTCCAATCCTACTGTTGCT and reverse primer was TCCCCGTCACCTCCAATCC; and the forward primer for GAPDH was TGACTTCAACAGCGACACCCA, and the reverse primer was CACCCTGTTGCTGTAGCCAAA. 2-ΔΔCt was utilized for the calculation of relative gene expression.

2.12 Western blot analysis of MMP2 and MMP3 after treatment with TMZ

U87MG tumor cells were cultured in vitro and treated with different concentrations of TMZ. The protein was extracted and western blot analysis for the anti-mouse MMP2 (Abcam, ab86607) 1: 1000, anti-rabbit MMP3 (CST, #14351) 1: 1000 and anti- mouse β-tubulin (Santa Cruz, SC-69879) 1: 2000 was performed. Secondary antibodies were rabbit IgG (Santa Cruz, sc-2004) and mouse IgG (Santa Cruz, sc-2005) 1: 5000.

2.13 Histology and immunohistochemistry

Mice were sacrificed after the imaging experiment, and the brain and tumor tissues were excised, fixed, and they were processed for paraffin embedding by a standard procedure. All sections which included glioma cells were used for histology and immunohistochemistry. Continuous sections (4 μm) were obtained, and preceded for hematoxylin and eosin (H&E) staining. For immunohistochemistry, tissue sections (thickness of 8 μm) were immunostained using anti-mouse MMP2 (Abcam, ab86607) and anti-rabbit MMP3 (CST, #14351) antibodies.

2.14 Statistical analysis

The experimental data were performed using Prism 5.0 (San Diego, CA, USA). Statistical analysis was calculated using the Student's t-test (two-tailed). The significance of differences in groups was compared using Tukey-Kramer's Multiple Comparison test. Data are represented as the mean ± SEM. In all tests, statistical significance was assumed to be $p<0.05$.

3. Results

3.1 Monitoring the anti-tumor efficacy of TMZ on the in vivo *gioma tumor model*

The anti-glioma therapeutic effects of TMZ were analyzed on subcutaneous and orthotopic glioma mouse models by measuring the BLI and tumor volume for 20 continuous days during treatment. In the glioma xenograft tumor model, BLI imaging in Fig. 2(a) showed that the BLI light signal increased rapidly in the control group, but the BLI light signal decreased during TMZ treatment suggesting that TMZ can effectively inhibit tumor growth during the observation period. As shown in Fig. 2(b), the tumor volume was also measured and the data were consistent with the *in vivo* BLI observation confirming the treatment efficacy of TMZ. The mouse body weight was measured and we did not observe significant weight loss suggesting that the dosing regimen of TMZ was well tolerated for the tumor bearing mice. Moreover, mouse survival was monitored, and the prolongation of mouse survival was found in the TMZ treatment group compared to the control group.

Biomedical Optics EXPRESS

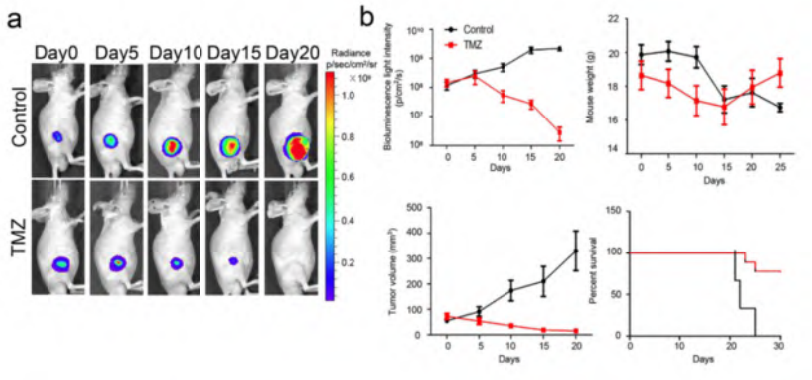

Fig. 2. The anti-glioma therapeutic effects of TMZ for the subcutaneous glioma mouse model. (a) BLI imaging of the TMZ treatment group and control group. (b) Bioluminescence light intensity, mouse body weight, tumor volume and percent survival of the TMZ treatment group and control group.

Based on the above observation, the orthotopic glioma mouse model was set up, and the TMZ treatment effects were observed (Fig. 3). BLI imaging showed that the BLI light signal decreased in the TMZ treatment group compared to the control group, which was confirmed by the measurement of BLI light intensity. Mouse survival was also elongated in the TMZ treatment group compared to the control group. To further confirm the *in vivo* BLI observation, MRI was also performed and we can find that the tumor volume was smaller in the TMZ treatment group compared to the control group, which was eventually confirmed by histology staining.

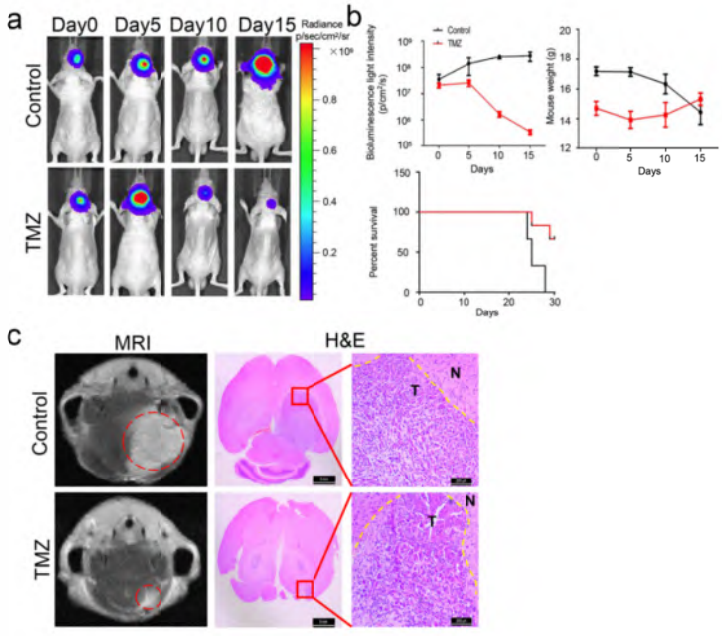

Fig. 3. The evaluation of TMZ treatment effects of the orthotopic glioma mouse model using bioluminescence imaging (BLI). (a) BLI of the TMZ treatment and control groups. (b) BLI light intensity, mouse body weight and percent survival of the TMZ treatment group and control group. (c) MRI and histology staining of the mouse glioma in the TMZ treatment group and control group.

Biomedical Optics EXPRESS

3.2 Evaluation of the chemotherapeutic response to TMZ treatment using BLT

For the orthotopic glioma mouse model, we cannot measure the tumor volume and also BLI imaging can only give us two dimensional information of tumors. In order to further analyze the antitumor efficacy, BLT was required to provide accurate results of tomographic reconstruction and localization of brain tumors in 3D visualization and also the tumor volume changes. Figure 4(a) and 4(a) represent the BLT data from the control and TMZ treatment groups, respectively. The reconstructed source distribution is shown in Fig. 4(a) and 4(e) from three different angles, including the transverse slice (Fig. 4(b), (f)), coronal slice (Fig. 4(c), (g)) and sagittal slice (Fig. 4(d), (h)). Comparing Fig. 4(a) with Fig. 4(b), we found that the tumor volume of the gliomas in the TMZ group was smaller than the control group. The BLT results confirmed that the growth of orthotopic gliomas in the TMZ group was greatly inhibited compared to the control group. The drug treatment efficacy of TMZ could be reliably assessed on gliomas through the BLT imaging method.

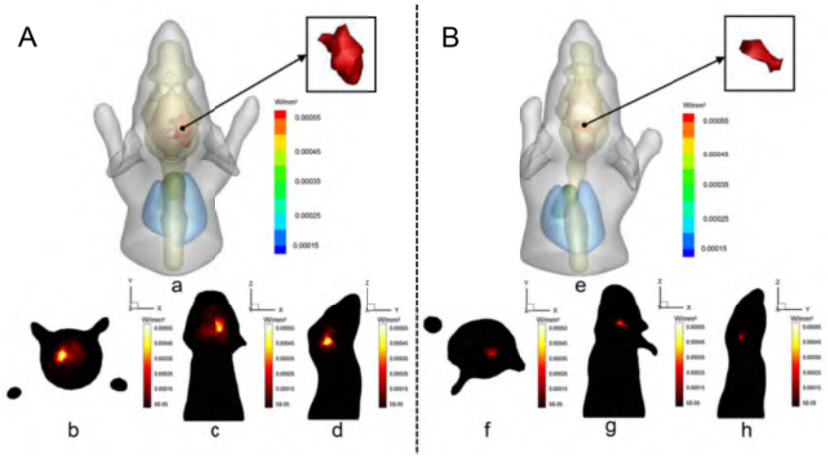

Fig. 4. BLT from the control and TMZ treatment groups. The reconstructed source distribution is shown in (a, e) from three different angles, including the transverse slice (b, f), coronal slice (c, g) and sagittal slice (d, h).

3.3 In vivo *MMP-750 bio-distribution*

The specific glioma targeting effect of MMP-750 was confirmed in our previous work (data not published), suggesting that MMP-750 is a smart probe for targeted glioma imaging. In this study, the fluorescence expression level of the MMP-750 probe was examined on both subcutaneous and orthotopic human U87MG gliomas with TMZ treatment using FMI at different time points after the injection of MMP-750. The tumor location was indicated by BLI in Fig. 5(a), 5(b). For the control group shown in Fig. 5(c), the fluorescence signal of MMP-750 at the tumor site increased gradually from 1 to 24 h post-injection and the FMI revealed good glioma targeting effects. The fluorescence signal was retained for at least 36 h post-injection, and then the fluorescence intensity decreased thereafter during the observation period. While for the TMZ treatment group, the fluorescence signal of MMP-750 was relatively weaker compared to the control group (Fig. 5(d)). The tumor-to-background ratio (TBR) of FMI was further measured and calculated, and the data in Fig. 5(e) show that the TBR of MMP-750 in the control group was relatively higher. Moreover, after the *in vivo* observation, tumors and also major organs were dissected out for further FMI imaging (Fig. 5(f)), and the results confirmed that MMP-750 was highly expressed in the control group compared to the TMZ group.

Biomedical Optics EXPRESS

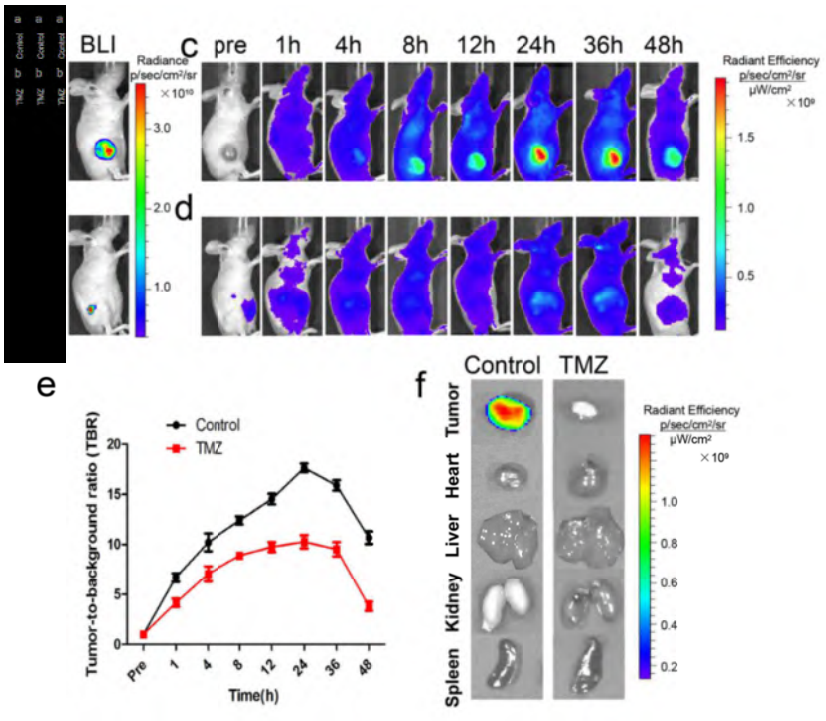

Fig. 5. The fluorescence expression level of MMP-750 probe on subcutaneous human U87MG glioma with TMZ treatment. (a) and (b) The tumor location via BLI. (c) and (d) The fluorescence signal of MMP-750 of the control group and the TMZ treatment group at different time points. (e) The tumor to background ratio (TBR) of FMI. (f) The *ex vivo* FMI imaging of the tumors and other major organs.

FMI imaging of MMP-750 on the orthotopic glioma mouse model with TMZ treatment was further examined using FMI. The orthotopic glioma mouse model preserves the maximum extent of the "natural" micro-environment of cancer [36, 37]. BLI denotes the glioma location in the brain of tumor-bearing mice (Fig. 6(a), (b)). For the control group shown in Fig. 6(c), the fluorescence signal in the tumor area was observed 1 h post-injection, and then gradually increased. The fluorescence signal at the brain tumor area reached a peak 24 h post-injection. The signal then gradually declined thereafter till 48 h. For the TMZ treatment group (Fig. 6(d)), the MMP750 fluorescence signal was relatively lower compared to the control group during the whole period of *in vivo* observation, which was consistent with the subcutaneous glioma mouse model. The TBR of FMI was consistent with the *in vivo* FMI observation, and the data in Fig. 6(e) show the highest FMI TBR of MMP-750 in the control group compared to the TMZ treatment group. Tumors and major organs of the mice were dissected 48 h post-injection for further FMI imaging. As shown in Fig. 6(f), the fluorescence signal of the glioma in the brain in the control group was higher than the signal of the glioma in the brain in the TMZ group, and almost no observable fluorescence signal was present in the other organs between animal groups. On the whole, MMP-750 exhibited a relatively lower fluorescence expression level compared to the control group suggesting the expression level of MMP-750 was correlated with the treatment efficacy of TMZ and MMP-750 expression level may predict the treatment effects.

Biomedical Optics EXPRESS

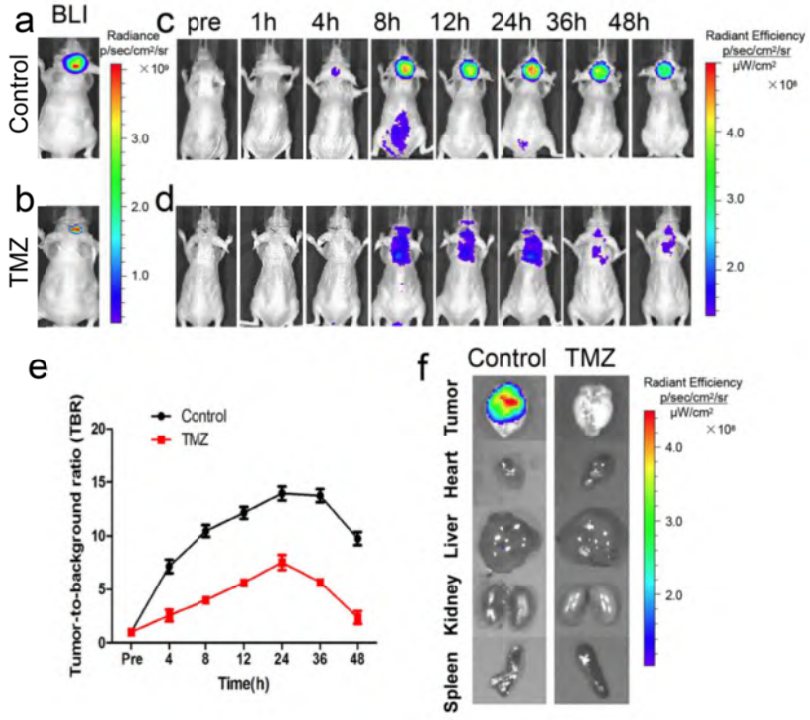

Fig. 6. The fluorescence expression level of the MMP-750 probe on orthotopic human U87MG glioma with or without TMZ treatment. (a) and (b) The glioma location in the brain of tumor-bearing mice via BLI. (c) and (d) The fluorescence signal of MMP-750 of the control group and the TMZ treatment group at different time points. (e) The tumor to background ratio (TBR) of FMI. (f) FMI imaging of tumors and other major organs of the mice.

3.4 MMP2 and MMP3 are involved in TMZ treatment

MMP750 smart probe represents a family of MMP members including MMP2, 3, 7, 9, 12 and 13. The decreased fluorescence signal of MMP-750 prompted us to further test which specific MMP members are involved in the regulation of TMZ treatment effects. MMP members were screened and we found that MMP2 and MMP3 were down-regulated after treatment with TMZ at both RNA and protein levels in in vitro experiments (Fig. 7). To further confirm the in vitro observation, *in vivo* tumor xenografts after treatment with TMZ were preceded for immunohistology and western blot staining of MMP2 and MMP3 (Fig. 8). The immuno-histological and western blot results showed that MMP2 and MMP3 were relatively lower expressed in TMZ treated tumors compared to control tumors suggesting that the chemotherapeutic effects of TMZ are possible through down-regulation of MMP2 and MMP3.

Biomedical Optics EXPRESS

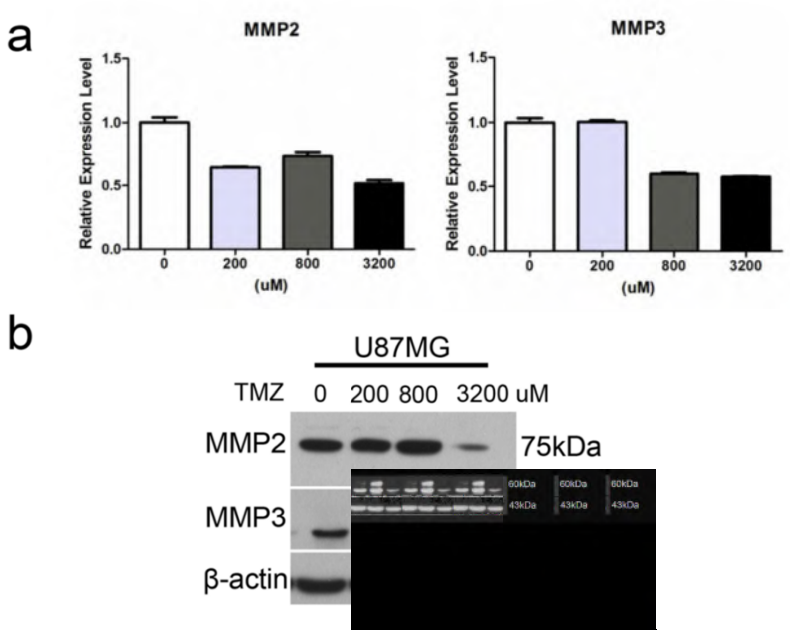

Fig. 7. MMP2 and MMP3 at both RNA and protein levels after treatment with TMZ in *in vitro* experiments.

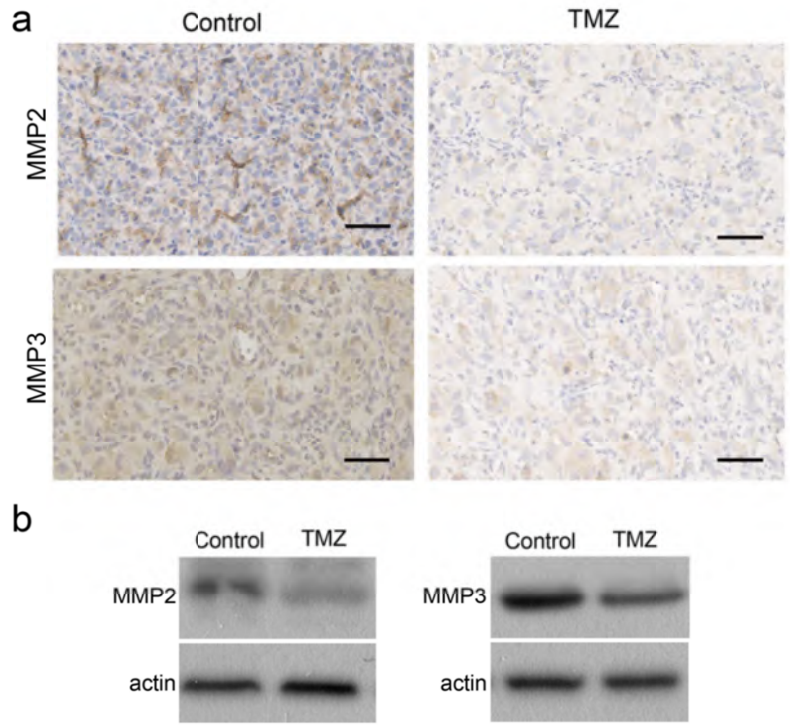

Fig. 8. The immunohistology and western blot staining of MMP2 and MMP3 for mouse glioma xenografts after treatment with TMZ.

Biomedical Optics EXPRESS

4. Discussion

In this work, we found that it is feasible to effectively evaluate the therapeutic effects of TMZ at the early stage using bioluminescence tomography (BLT). At the same time, the smart MMP-750 probe can be used to predict the antitumor activities of TMZ therapy. Finally, the expression of MMP2 and MMP3 may be involved in the regulation of therapeutic effects of TMZ.

BLI is an ideal *in vivo* imaging method to observe the biological behavior of the tumor and assess the drug therapeutic efficacy at cellular levels. Edinger et al. revealed lymphoma growth and the efficacy of immune cell therapies using *in vivo* BLI [38]. The experiments of Folaron et al. showed the safety and efficacy of the vascular disrupting agent in experimental glioma models using BLI and MRI [39]. Galiger et al. assessed the efficacy of antifungals against Aspergillus fumigatus using BLI [40]. In this study, we evaluated the antitumor efficacy of TMZ treatment using BLI. It showed that TMZ effectively inhibited glioma growth in both subcutaneous and orthotopic human U87MG-fLuc glioma animal models. MRI and HE histology confirmed the *in vivo* BLI observation.

Second, a multi-modality imaging method was utilized to make a more comprehensive assessment of TMZ treatment on gliomas. BLT utilizes *in vivo* optical imaging technology and mathematical modeling to produce three dimensional (3D) bioluminescent images. In combination with the bioluminescent signal of the mouse surface, we propose the reconstruction process of light sources using the ASMP method, which could provide 3D tumor volume information. Hence, we can evaluate drug treatment efficacy of TMZ more accurately and comprehensively with BLT. The results demonstrated that TMZ can effectively inhibit tumor growth and the feasibility of our methodology for localization and quantification of the optical imaging *in vivo*. It can contribute to the early diagnosis and better treatment of cancer, and thereby substantially improving health-related quality of life.

Third, the expression level of the MMP-750 probe was examined on both subcutaneous and orthotopic human U87MG gliomas with TMZ treatment using FMI. MMPs are key proteolytic enzymes of tumor invasion and metastasis [41, 42]. Based on their extracellular matrix degradation capacity in the extracellular mediators of various tissues, MMPs can regulate tumor invasion and metastasis [43–47]. So we hypothesize that the expression of smart MMP-750 probes in the glioma can help predict antitumor activities of TMZ therapy. Our experimental results showed that the targeted imaging of MMP-750 was decreased in the glioma after treatment with TMZ compared with the control group. Our experimental results proved the above statement.

Finally, MMP members were screened after treatment with TMZ. The results showed that MMP2 and MMP3 expression was relatively decreased in the TMZ-treated group compared to the control group suggesting that the chemotherapeutic effects of TMZ are possible through down-regulation of the expression of MMP2 and MMP3, which has a marked impact in tumor invasion and metastasis in both physiological and pathological processes of brain cancer.

Our future work will focus on combining multiple imaging modalities, such as fluorescence molecular tomography (FMT), magnetic resonance imaging (MRI) and positron emission tomography (PET), to comprehensively assess the anti-tumor efficacy of TMZ or other drugs for glioma treatment to provide early prediction and assessment of therapeutic effects. Moreover, we will try to utilize the intelligent MMP fluorescence probe for targeted glioma imaging in clinical trials. At the same time, more work should focus on the in-depth molecular mechanism study of MMPs to provide a deeper understanding of the roles of MMPs in glioblastoma. The smart MMP-750 probe we used in this study is currently for research only. More experiments and safety evaluation will be made for the MMP-targeted fluorescence probes to pass FDA requirements for future clinical application.

Biomedical Optics EXPRESS

Funding

Ministry of Science and Technology of China (2017YFA0205200, 2014CB748600, 2015CB755500); National Natural Science Foundation of China (81470083, 81227901, 81527805, 81571810, 81771846); the Research and Development Program of China (973) (2014CB748600 and 2015CB755500); Chinese Academy of Sciences (GJJSTD20170004).

Acknowledgments

All authors would like to thank Ms. Yuan Li and Ms. Ting Sun from Peking Union Medical College Hospital, Beijing, China for animal handling assistance. The authors thank Dr. Jinzuo Ye from CAS Key Laboratory of Molecular Imaging, Institute of Automation, Chinese Academy of Sciences, Beijing, China for his assistance in conducting the experiments of our multimodality system. The authors also would like to thank Adjunct Assistant Professor Dr. Karen M. von Deneen from the University of Florida for her English editing of this paper.

Disclosures

The authors declare that there are no conflicts of interest related to this article.